

Direct Numerical Simulations and Experiments of Turbulence Over Regular Roughness From the Transitionally Rough to the Fully Rough Regime

Hiten Mulchandani ^{*}, Melissa J. Adams [†], and Ricardo García-Mayoral [‡]
University of Cambridge, Cambridge CB2 1PZ, UK

Vidya Vishwanathan [§], Daniel J. Fritsch [¶], K. Todd Lowe ^{||}, and William Devenport ^{**}
Virginia Tech, Blacksburg, VA 24061

We present results of experiments and fully resolved, direct numerical simulations (DNSs) on turbulent flows over regular arrays of cylindrical roughness elements. The experimental campaign was conducted in the Virginia Tech Stability Wind Tunnel for $k^+ \approx 225 - 400$ at $Re_\tau \approx 7110 - 16700$, where the ‘+’ superscript represents wall-unit scaling with kinematic viscosity and the friction velocity. DNSs were conducted for $k^+ = 5, 10, 15$, and 20 at $Re_\tau \approx 190$ and for $k^+ = 20$ at $Re_\tau \approx 380$. Data from experiments and DNSs are presented and discussed for the roughness function, equivalent sand-grain roughness, mean flow velocity profiles, turbulence statistics, and spectral energy densities. Experimental results suggest the method used to estimate the equivalent sand-grain roughness from mean velocity profiles is sensitive to the selection of the logarithmic region considered in the regression fit, highlighting the need for an improved analytical method to estimate roughness parameters from the mean velocity profiles. DNS results suggest there is a progressive departure from smooth-wall-like turbulence for all cases except the smallest roughness size investigated. We hypothesise the differences are related to the nonlinear interaction of the texture-coherent flow with the background turbulence and plan to assess the importance of this mechanism in future work.

I. Nomenclature

d	=	Roughness element diameter
k^+	=	Roughness element height in wall units
k_s^+	=	Equivalent sand-grain roughness in wall units
ℓ_T^+	=	Virtual origin of turbulence in wall units
Re_τ	=	Frictional Reynolds number
s	=	Roughness element spacing
U^+	=	Mean streamwise velocity in wall units
U_e	=	Boundary layer edge velocity
ΔU^+	=	Roughness function in wall units
ΔU_m^+	=	Roughness function measured from DNSs in wall units
u'^+	=	Streamwise velocity fluctuations in wall units
v'^+	=	Wall-normal velocity fluctuations in wall units
w'^+	=	Spanwise velocity fluctuations in wall units
y	=	Wall-normal direction
τ_w	=	Wall shear stress

^{*}Graduate Research Assistant, Department of Engineering, University of Cambridge.

[†]Graduate Research Assistant, Department of Engineering, University of Cambridge.

[‡]Associate Professor, Department of Engineering, University of Cambridge.

[§]Graduate Research Assistant, Crofton Department of Aerospace and Ocean Engineering, AIAA Student Member.

[¶]Graduate Research Assistant, Crofton Department of Aerospace and Ocean Engineering, AIAA Student Member.

^{||}Professor, Crofton Department of Aerospace and Ocean Engineering, AIAA Associate Fellow.

^{**}Crofton Professor, Crofton Department of Aerospace and Ocean Engineering, AIAA Associate Fellow.

II. Introduction

MANY engineering surfaces are rough and cause additional drag compared to smooth surfaces, and it is of industrial interest to quantify this drag. Sufficiently far above the roughness elements, it is commonly accepted that smooth- and rough-wall turbulence behave in a similar manner in what is known as outer-layer similarity [1, 2]. The effect of the roughness reduces, then, to an offset in the mean velocity profile of a rough wall relative to that of a smooth wall. This is given by the roughness function, $\Delta U^+ = U_S^+ - U_R^+$, where the superscript ‘+’ indicates wall-unit scaling with kinematic viscosity and the friction velocity, and the subscripts ‘S’ and ‘R’ indicate smooth and rough walls, respectively. Defining the skin-friction coefficient as $C_f = \tau_w / (\rho U_\delta^2 / 2) = 2 / U_\delta^{+2}$, the impact of ΔU^+ on C_f through the decrease in U_δ^+ for rough walls becomes immediately apparent [3]. When expressed in wall units, ΔU^+ is generally believed to be independent of the Reynolds number for a given roughness geometry and size, k^+ [4]. In turn, the change in C_f depends on the Reynolds number through the reference smooth U_δ^+ . The offset increases with k^+ , but how it varies greatly depends on the roughness geometry and thus it is difficult to predict *a priori* [3, 5]. To circumvent this difficulty, an equivalent “sand-grain roughness,” k_s^+ , is often employed to characterize the effect of the surface, so that the actual surface is referred to the sand-grain surface that produced the same ΔU^+ in the pioneering experiments of Nikuradse [6]. This, however, simply transfers the problem from predicting ΔU^+ to predicting k_s^+ , as there is a one-to-one relationship between both quantities. Furthermore, the ratio k_s/k for a given surface only becomes constant in the fully rough regime [3, 5], when it becomes equal to $k_{s,\infty}/k$ and the curve $k_{s,\infty}^+ - \Delta U^+$ becomes universal. It is therefore important to understand the physical mechanisms at play in determining ΔU^+ or k_s^+ , up to the roughness size for which the flow becomes fully rough. Beyond this point, the practical interest in understanding the physical mechanisms is more limited.

Toward this aim, we conduct experiments and fully resolved, direct numerical simulations (DNSs) of turbulent flows over regular arrays of cylindrical roughness elements. The roughness function varies from small roughness (i.e., hydraulically smooth) to the onset of the transitionally rough regime through to the fully rough regime. When the roughness is much smaller than the smallest eddies in the near-wall flow, the overlying turbulent flow perceives the near-wall flow to be smooth-wall-like and the roughness is perceived as a homogenised boundary condition by the overlying flow [7]. As the roughness size becomes comparable to the size of the near-wall turbulent eddies, the overlying flow begins to perceive the non-homogeneity of the texture. However, in the context of alternating slip/no-slip patterns for superhydrophobic surfaces, Fairhall et al. [8] observed that the overlying flow still perceived a homogenised boundary condition from the surface up to $k^+ \approx 50$, but noted that the texture caused additional dissipation in the flow above from $k^+ \approx 15$. Fairhall et al. [8] proposed that this additional dissipation was caused by the nonlinear interaction between the texture-induced flow and the background turbulence. We aim to assess the importance of this mechanism for roughness, and ultimately to aid in the development of physics-based models that can predict ΔU^+ *a priori* without resorting to costly experiments, simulations, or correlations (if available) to similar surfaces. This work is part of the activity of NATO’s Research Task Group Air Vehicles Technology (AVT) 349, and focuses on the canonical effect of roughness in equilibrium conditions.

This paper is a preliminary presentation of the results – comparisons between the experimental and numerical results will be presented in future work. It is organised as follows. In Sec. III, we outline the experimental and numerical methods used in the investigation. Results for the roughness function, equivalent sand-grain roughness, turbulence statistics, and spectral energy densities are presented and discussed in Sec. IV. Finally, Sec. V summarises the work and concludes the paper.

III. Methodology

A. Experimental Methods

The experimental campaign was conducted in the Virginia Tech Stability Wind Tunnel. The test section is 7.3 m long with a 1.85 m x 1.85 m square cross section. The side walls consist of 0.61 m x 0.61 m modular square panels, carefully levelled to produce a continuous surface, arranged in a grid pattern that can be removed and replaced with panels with custom instrumentation. All measurements were conducted on the port-side test-section wall (the lower wall shown in Fig. 1), which was covered in a staggered pattern array of cylindrical roughness elements, as shown in Fig. 2. Each element is 2 mm tall and 3.14 mm in diameter, corresponding to $k^+ \approx 225 - 400$. To ensure the flow is fully turbulent when it enters the test section, the boundary layer is tripped on all four walls of the contraction section. The roughness fetch starts at a streamwise position that is 3.58 m downstream of this boundary layer trip. The upstream edge of the roughness fetch serves as the coordinate system origin of the experimental setup as shown in Fig. 1. The ratio of element spacing to its height was fixed at $s/k = 3.46$ and the ratio of element diameter to its

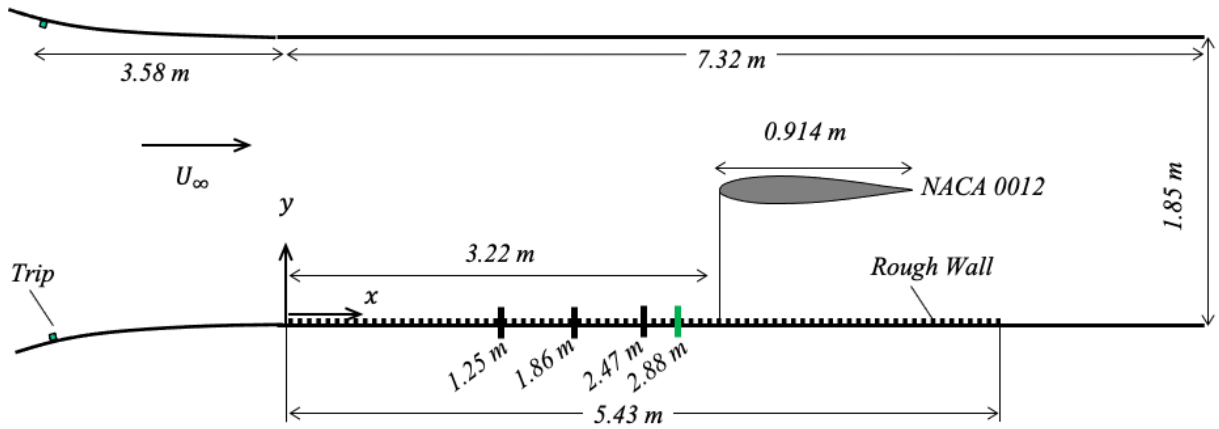


Fig. 1 Top-down schematic of the test section used in the experimental campaign. The lower wall is covered in cylindrical roughness elements. The mean velocity data were measured at three streamwise stations (black lines) upstream of a NACA 0012 airfoil at 0° angle of attack, where the flow is at nominally zero-pressure gradient. The location of rough wall turbulence stress measurements using TR-PIV is shown in green.

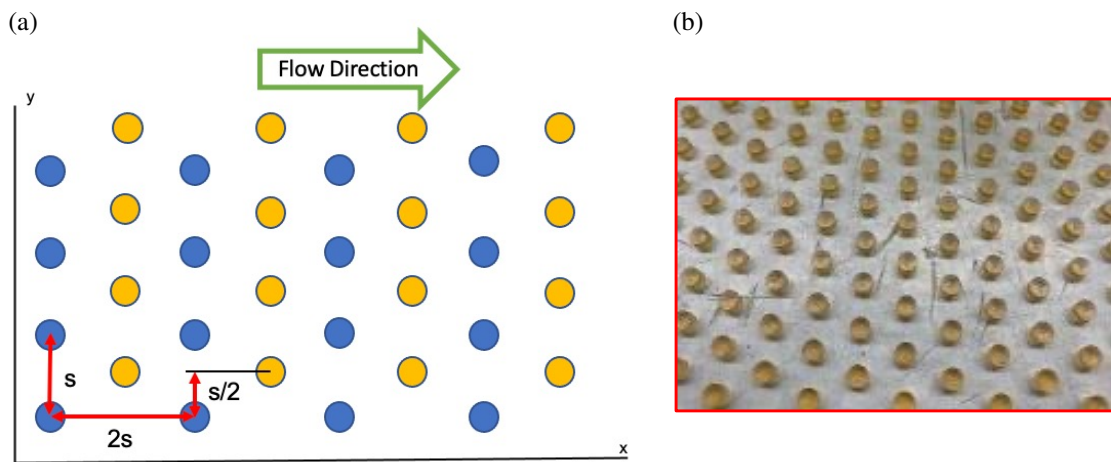


Fig. 2 (a) Schematic of staggered cylindrical roughness elements and, (b) as fabricated and on the modular panels used in the experimental configuration.

spacing was fixed at $d/s = 0.45$. Experimental data were measured at 2.18 million and 3.83 million Reynolds numbers per meter, corresponding to $Re_\tau \approx 7110 - 16700$ and inflow boundary layer thicknesses of 62.2 mm and 59.44 mm respectively. These flow conditions produce a roughness Reynolds number ranging between $k_s^+ \approx 380 - 680$. This flow is therefore in the fully rough regime. A NACA 0012 airfoil was positioned at the center of the test section and was rotated to specified angles of attack to induce a systematic variation of pressure gradient on the side walls. To separate the roughness impacts from pressure gradient effects on the turbulent boundary layer, we discuss data acquired at nominally zero-pressure gradient (i.e., the airfoil is positioned at 0° angle of attack).

The experimental mean velocity data were acquired using a 30-Pitot probe boundary layer rake (for which smooth wall results and instrument specifications are described in further detail in Fritsch et al. [9] and Vishwanathan et al. [10]). The boundary layer rake was mounted on the modular test section wall panels and moved to several streamwise positions. The mean velocity profiles measured at the three upstream measurement locations are investigated, located at 1.97 m, 1.36 m, and 0.75 m upstream of the airfoil leading edge, as indicated in Fig. 1. Turbulence statistics were measured using 2D, three component (2D3C) time-resolved particle image velocimetry (TR-PIV). The data were processed in LaVision's DaVis10 using two initial passes of a 64×64 pixel² interrogation window with 50% overlap, which was followed by two final passes of a 24×24 pixel² interrogation window with a 75% overlap. This corresponded to a spatial resolution of 0.57 mm. A laser-sheet was emitted from the boundary layer wall using a Photonics Nd:YAG dual cavity diode pumped solid state, high repetition rate laser emitting 532 nm light at 15 mJ/pulse. A Phantom v2512 camera recorded 24,839 realizations in double-frame mode at a low sampling rate of 1kHz and a high-speed rate of 12.85 kHz. Only the turbulence data measured at a location 0.34 m upstream of the airfoil are discussed in this paper.

B. Numerical Methods

We conduct DNSs of incompressible flow in a periodic channel driven by a constant mean pressure gradient with roughness on the top and bottom walls, imposed using immersed boundaries, using a code adapted from Sharma and García-Mayoral [11] and Sharma and García-Mayoral [12]. The channel is of size $2\pi\delta \times 2(\delta + k) \times \pi\delta$ in the streamwise, wall-normal, and spanwise directions, respectively, where δ is the channel half-height from the tips of the roughness to the center of the channel and k is the roughness height. A spectral discretisation is employed in the streamwise and spanwise directions and a second-order central difference scheme on a staggered grid is employed in the wall-normal direction. The grid is stretched such that $\Delta y_{min}^+ \approx 0.4$ near the walls and $\Delta y_{max}^+ \approx 4$ in the center. The code uses a 'multiblock' grid which allows finer resolution near the walls compared to the channel center to properly resolve the flow between the roughness elements. At the center of the channel, the grid resolution is standard for DNSs, with $\Delta x^+ \leq 8$ and $\Delta z^+ \leq 4$. Near the walls, the resolution in the streamwise and spanwise directions is 24 grid points for a periodic box containing one roughness element, except the smallest case studied, $k^+ = 5$, for which the resolution is 12 grid points. Time integration is carried out using a three-step Runge–Kutta scheme with a fractional step, pressure correction method that enforces continuity [13], for which the time-step is set by a fixed advective CFL number of 0.7.

IV. Results

A. Experimental Results

1. Skin Friction & Roughness Parameters

The analytical methods to determine skin-friction from the Law of the Wall as described by Perry and Joubert [14] were used to compute skin-friction and the roughness function from the experimental mean velocity profiles. In this method, the Law of the Wall for rough surfaces is rearranged in terms of the velocity normalized on the boundary layer edge velocity, U_e , such that the slope and intercept of the curve are functions of the skin-friction and roughness function,

$$\frac{U}{U_e} = m \ln y + P, \quad (1)$$

where the slope is in terms of the skin-friction coefficient given by

$$m = \frac{1}{\kappa} \sqrt{\frac{C_f}{2}}, \quad (2)$$

and the intercept is given by

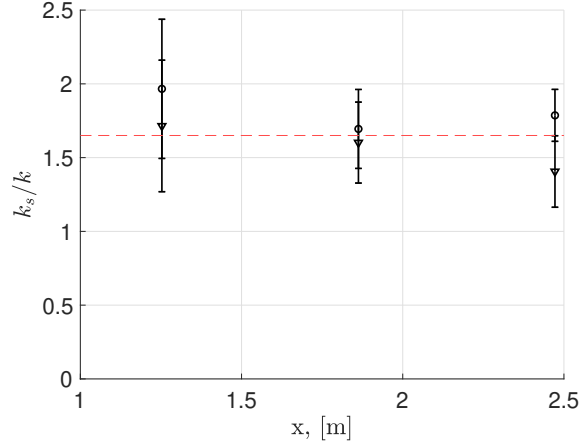


Fig. 3 k_s/k versus streamwise position determined from regression fit of the logarithmic region of the mean velocity profiles. Data at a Reynolds number per meter of 2.18 million are shown as (○) and 3.85 million is shown as (▽). Red dashed line (- - -) indicates a constant $k_s/k = 1.65$.

$$P = \sqrt{\frac{C_f}{2}} \left(\frac{1}{\kappa} \ln \left[\frac{U_e}{\nu} \sqrt{\frac{C_f}{2}} \right] + C - \Delta U^+ \right). \quad (3)$$

The von Kármán constant, κ , and the log-law intercept, C , are taken to be 0.41 and 5.0, respectively, and the logarithmic region of the mean velocity profiles is fit using a regression line. The slope of this line is used to compute the skin-friction, which is then input into a rearranged form of the slope-intercept equation, P , to determine the roughness function. Nikuradse's [6] effective sand-grain roughness is calculated from the roughness function by

$$\Delta U^+ = \frac{1}{\kappa} \ln(k_s^+) - 3.5. \quad (4)$$

The equivalent sand-grain roughness values derived from this method are sensitive to the selection of the data points within the logarithmic region used in the regression fit. The logarithmic region was selected based on inspection of the velocity profiles plotted on a semi-logarithmic axis along the wall-normal position. A sensitivity study of the logarithmic region selection on the k_s distribution revealed that for the boundary layer profiles measured at the three streamwise locations upstream of the airfoil in nominally zero-pressure gradient, the k_s values, normalized by the roughness height k , could vary anywhere between $1.16 < k_s/k < 2.16$. These uncertainty bands suggest that any variation in k_s with streamwise position is not necessarily a functional response to the flow, but rather a sensitivity to the selection of the logarithmic region considered in the fit method. By evaluating the relative magnitudes of the shear velocity development in streamwise position, we estimate a $k_s/k \approx 1.65$ to be representative of the rough wall flow conditions. Considering the uncertainty bands of Fig. 3, this constant value is justified.

2. Mean Statistics

The mean velocity profiles are shown in Fig. 4 in defect and inner coordinates. The effect of the roughness is to increase the frictional stresses on the mean velocity resulting in a downward shift of the profiles which is captured in the roughness function. However, the logarithmic portion for all profiles collapse, satisfying the Law of the Wall. The profiles normalized by wall coordinates make clear the comparatively larger wake region in the rough wall configuration and an enlarging wake with increasing Reynolds number and subsequent downstream development.

Turbulence stresses from the rough wall configuration are plotted against the smooth wall profiles in Fig. 5. The smooth wall data were measured using a planar PIV configuration, as described in Vishwanathan et al. [10], therefore only two components of stresses are shown. The effect of the roughness is to increase the overall turbulence levels, especially in the vicinity of the roughness. An examination of the relative turbulence magnitudes and their contributions to sweeps and ejections is a topic of future study. Outer-layer similarity is demonstrated in inner-outer coordinates, evidenced by the collapse of the the $\overline{u^2}$ profiles beyond the vicinity of the roughness elements. It should be noted that

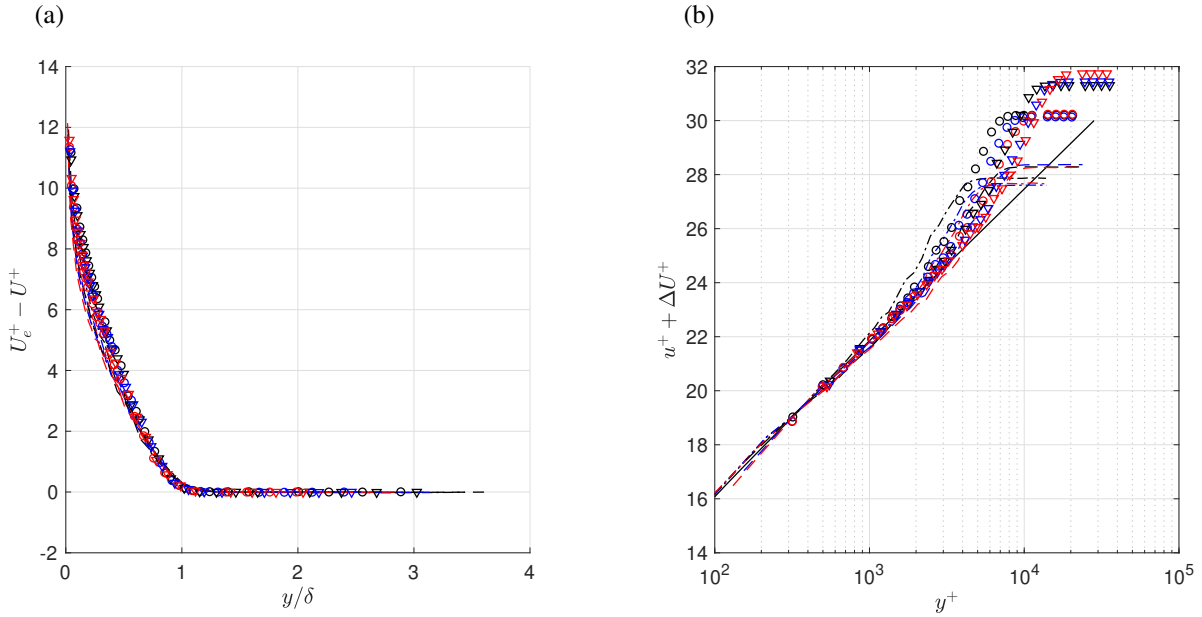


Fig. 4 Experimentally measured mean velocity profiles in (a) defect coordinates and (b) in wall coordinates. Data for Reynolds number per meter of 2.18 million comparing the smooth wall at locations $x = 1.25$ m (---), $x = 1.86$ m (- - -), $x = 2.47$ m (- . - .) with the rough wall at locations $x = 1.25$ (○) m, $x = 1.86$ m (○), $x = 2.47$ m (○). Data for Reynolds number per meter of 3.85 million comparing the smooth wall at locations $x = 1.25$ m (- - -), $x = 1.86$ m (- - -), $x = 2.47$ m (- . - .) with the rough wall at locations $x = 1.25$ (▽) m, $x = 1.85$ m (▽), $x = 2.47$ m (▽).

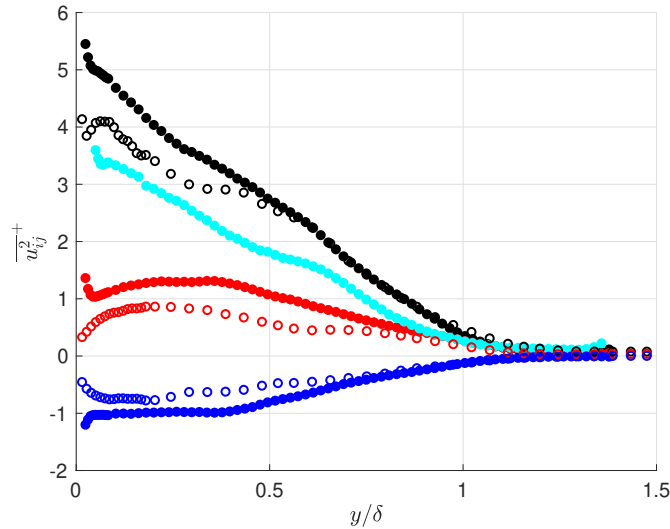


Fig. 5 Reynolds turbulence stresses measured at $x = 2.88$ m (rough wall) at 2.18 million Reynolds number per meter plotted on inner-outer coordinates for the rough (filled) and smooth wall (open); $\overline{u^2}^+$ (●), $\overline{v^2}^+$ (●), $\overline{w^2}^+$ (●), \overline{uv}^+ (●).

Table 1 Parameters from the cases studied.

k^+	Re_τ	ΔU_m^+	ℓ_T^+	U_t^+	$U_S^+(\ell_T^+)$
5	187	1.39	3.08	1.19	2.74
10	188	4.51	6.20	1.92	5.47
15	190	6.58	9.40	2.23	7.76
20	191	7.74	12.63	2.38	9.52
20	376	7.44	12.40	2.39	9.36

the smooth wall data were processed with a coarser spatial resolution (≈ 0.78 mm), which has the greatest impact on the resulting wall-normal (and by extension shear stress) turbulence magnitudes. The spatial resolution particularly affects near wall turbulence representation, thus wall similarity may actually extend further into the boundary layer than shown.

B. Numerical Results

Table 1 presents the parameters of the cases studied for different frictional Reynolds numbers, Re_τ , and roughness heights, k^+ . The same ratio of spacing to height and diameter to spacing was used for the cylindrical roughness elements as in the experimental campaign. The instantaneous flow realizations in Fig. 6 show simulation results over the texture geometry. The measured roughness function, ΔU_m^+ , is obtained from the DNSs by subtracting the rough-wall mean velocity profile from the smooth-wall mean velocity profile and averaging over the log layer. The measured roughness function against equivalent sand-grain roughness is shown in Fig. 7 for the cases studied, overlaid with values for other rough surfaces. A simulation at $k^+ = 40$ ($Re_\tau \approx 380$) is currently underway for which we expect ΔU_m^+ to lie in the fully rough regime, thereby unequivocally providing a full set of DNS data from the transitionally rough to the full rough regime.

We define $y^+ = 0$ at the plane of the roughness tips. For small roughness, $k^+ = 5$, turbulence is smooth-wall-like, except for an offset, ℓ_T^+ , such that it perceives an apparent ‘virtual’ origin at $y^+ = -\ell_T^+$ [15, 16]. Turbulence then remains essentially unchanged compared to that over a smooth wall, except for an offset given by the virtual origin. The physical argument for this is that the virtual origin for turbulence is where the quasi-streamwise vortices of the near-wall cycle perceive the wall, and this sets the origin perceived by the whole turbulence dynamics, as proposed by Luchini [15]. We find the value of the offset by fitting the curve representing the Reynolds shear stress to smooth-wall data. Likewise, the mean-flow virtual origin is the distance below the roughness tips at which the streamwise flow experiences an apparent, no-slip wall. We determine the virtual origin for the streamwise flow by extrapolating the mean velocity profile above the roughness tips to a depth below the tips where it would vanish. From the streamwise mean momentum equation, the Reynolds stress determines the shape of the mean velocity profile [17]. The Reynolds shear stress and the shape of the mean velocity profile would therefore be the same as for the flow over a smooth wall above $y^+ = -\ell_T^+$. At $y^+ = 0$, the value of the mean velocity is U_t^+ for the rough-wall flow, while it would be $U_S^+(\ell_T^+)$ for the reference smooth-wall flow. If the rough-wall flow follows that of the smooth-wall above $y^+ = 0$, both mean profiles would have the same shape but shifted by a constant offset given by $\Delta U^+ = U_S^+(\ell_T^+) - U_t^+$.

This estimated ΔU^+ is shown in Fig. 8 for $k^+ = 5$ to $k^+ = 20$ at $Re_\tau \approx 190$. For small roughness, $k^+ = 5$, there is good collapse of the mean streamwise velocity and the wall-normal and spanwise root mean square (r.m.s.) velocity fluctuations shifted by the virtual origin onto the smooth-wall profile. The streamwise r.m.s. velocity fluctuations profile does not collapse onto the smooth-wall profile near the wall. This is because the virtual origin for turbulence is essentially determined by the origin perceived by the quasi-streamwise vortices, which induce wall-normal and spanwise velocity fluctuations near the surface of the roughness tips [16]. In turn, the origin perceived by the near-wall streaks, associated with streamwise velocity fluctuations, plays at most a secondary role [16]. For larger roughness sizes, the near-wall cycle is more severely disrupted and turbulence is no longer smooth-wall-like, as evidenced by a lack of collapse of the data for $k^+ \geq 10$.

To analyze the effect of frictional Reynolds number on the mean velocity profile and turbulence statistics, we compare the results at $Re_\tau \approx 187$ with $Re_\tau \approx 376$ for $k^+ = 20$, in contrast with the results at $Re_\tau \approx 180$ with $Re_\tau \approx 360$ for smooth-wall data, as shown in Fig. 9. For smooth-wall data, the observed differences are consistent with changes observed in the frictional Reynolds number. For rough-wall data, the trends in the mean velocity profiles are very similar at the two frictional Reynolds numbers. Away from the roughness elements, at $y^+ > 50$, the Reynolds stresses from rough-wall simulations coincide with those from smooth-wall simulations at their corresponding frictional Reynolds

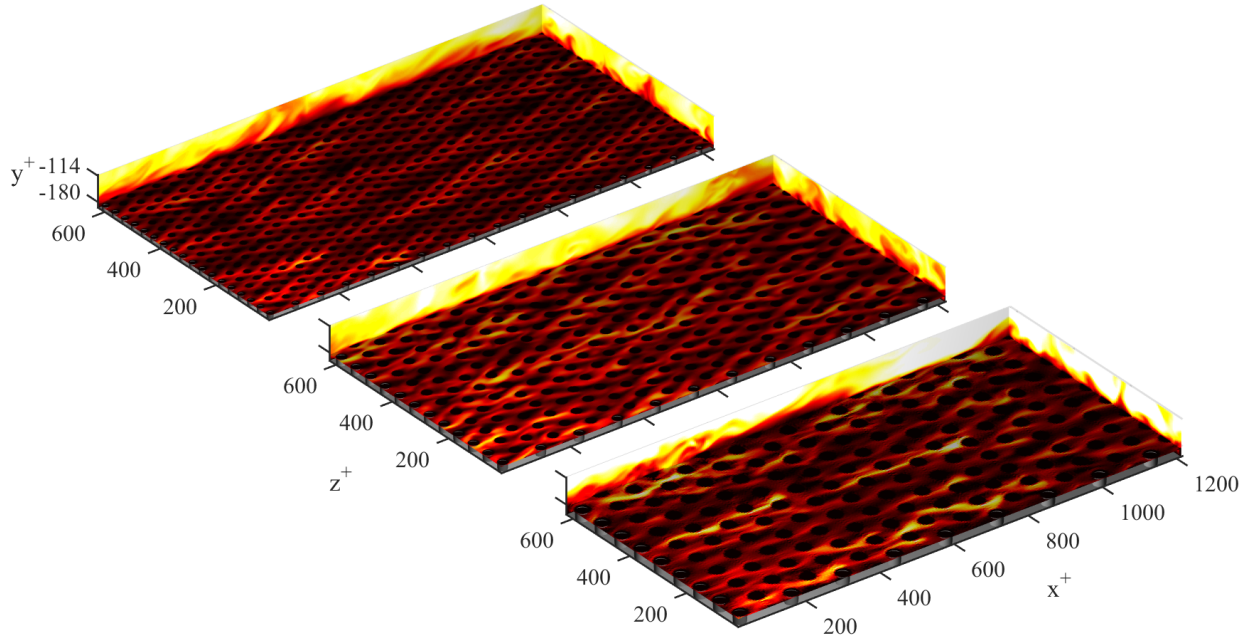


Fig. 6 Instantaneous realizations of the fluctuating streamwise velocity from the DNSs of a regular array of cylindrical roughness elements at $k^+ = 10, 15,$ and 20 at $Re_\tau \approx 190$.

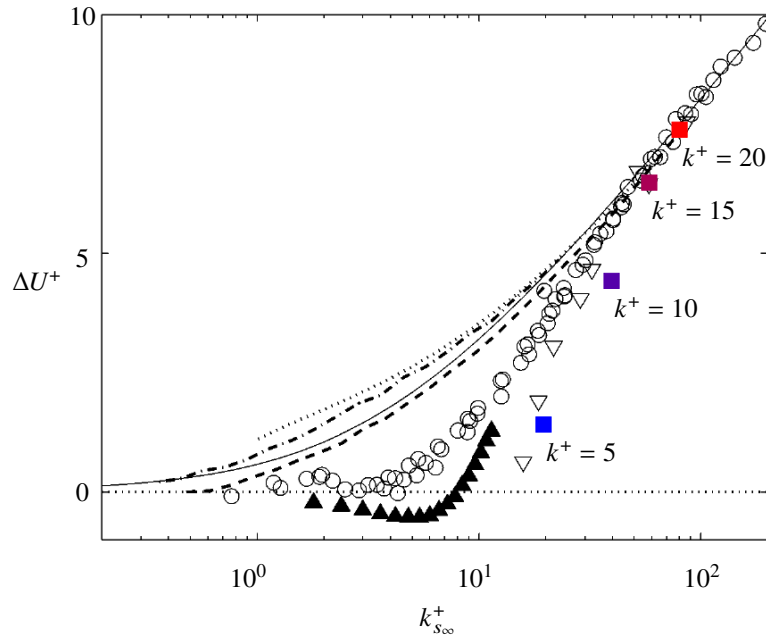


Fig. 7 Roughness function against equivalent sand-grain roughness for the present regular staggered cylinders (squares), compared with uniform sand (circles), uniform packed spheres (white triangles), galvanised iron (dotted line), tar-coated cast iron (dashed line), wrought iron (dotted dashed line), interpolation (solid line) and riblets (black triangles), adapted from [5].

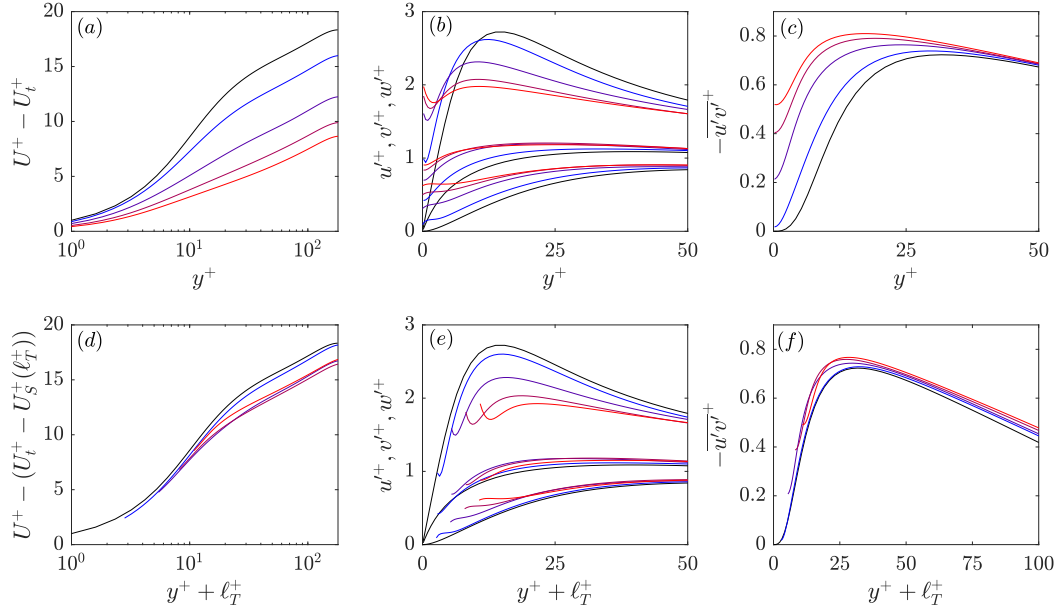


Fig. 8 Results from DNSs for $k^+ \approx 5$ (—), $k^+ \approx 10$ (—), $k^+ \approx 15$ (—), and $k^+ \approx 20$ (—) with $Re_\tau \approx 190$, and a smooth wall with $Re_\tau \approx 180$ (—) for (a) the mean streamwise velocity profile with the velocity at the tips subtracted, (b) r.m.s. velocity fluctuations, (c) Reynolds shear stresses, (d) mean streamwise velocity profile shifted by the turbulent virtual origin with the predicted velocity at the virtual origin subtracted, (e) r.m.s. velocity fluctuations shifted by the virtual origin, and (f) Reynolds stresses shifted by the virtual origin.

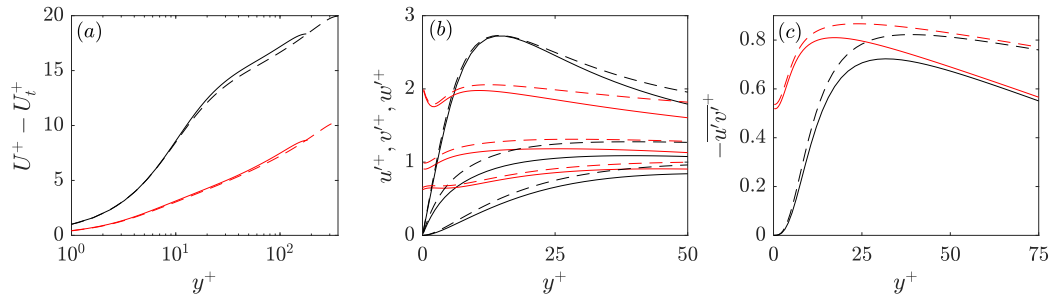


Fig. 9 Results from DNSs for $k^+ \approx 20$ with $Re_\tau \approx 187$ (—) and $Re_\tau \approx 376$ (- - -), and a smooth wall with $Re_\tau \approx 180$ (—) and $Re_\tau \approx 360$ (- - -) for (a) the mean streamwise velocity profile with the velocity at the tips subtracted, (b) r.m.s. velocity fluctuations, and (c) Reynolds shear stresses.

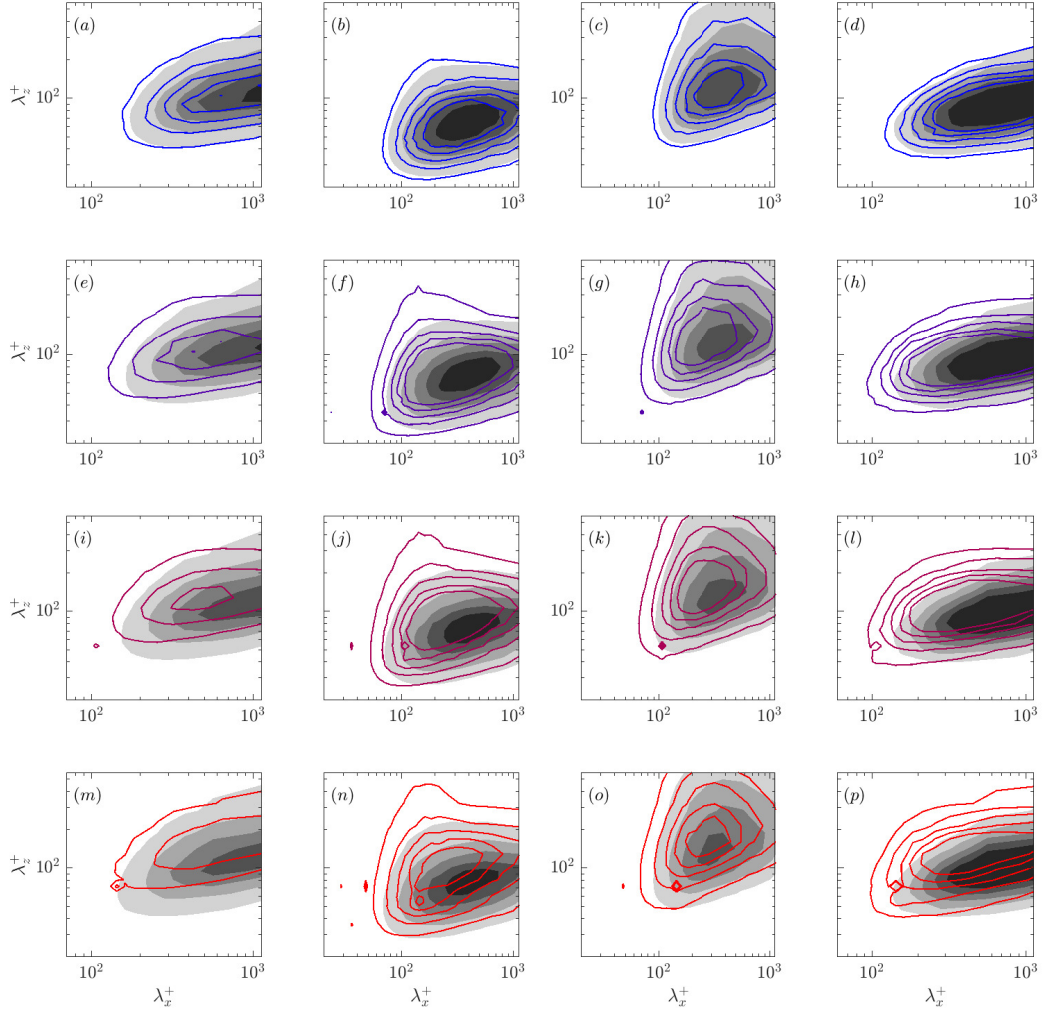


Fig. 10 Pre-multiplied two-dimensional spectral energy densities at $y^+ \approx 10$ of (a, e, i, m) $k_x k_z E_{uu}^+$, (b, f, j, n) $k_x k_z E_{vv}^+$, (c, g, k, o) $k_x k_z E_{ww}^+$, and (d, h, l, p) $-k_x k_z E_{uv}^+$. Results for $k^+ \approx 5$ (—), $k^+ \approx 10$ (—), $k^+ \approx 15$ (—), and $k^+ \approx 20$ (—) with $Re_\tau \approx 190$, and a smooth wall with $Re_\tau \approx 180$ (filled contours).

numbers, indicating the recovery of outer-layer similarity. Minor differences in the collapse are caused by small differences in the corresponding frictional Reynolds numbers. These arguments support the use of DNSs at a low frictional Reynolds number.

The spectral energy densities in Fig. 10 portray the distribution of energy across different length scales in the flow. There is a progressive departure from smooth-wall behaviour towards shorter wavelengths in the streamwise direction and wider wavelengths in the spanwise direction as the roughness height increases from $k^+ = 5$ to $k^+ = 20$. The effect of the surface texture on the flow is also evident from the concentration of energy at the roughness spacing and its harmonics from $k^+ = 10$ onward. As discussed above, it is hypothesised that the differences arise from extra Reynolds stresses resulting from the nonlinear interaction with the dispersive flow [8]. We are therefore interested in characterizing deviations from smooth-wall turbulence and the dispersive flow from this data.

V. Conclusions

In this paper, results from experiments and DNSs of turbulent flows over regular arrays of cylindrical roughness elements are presented and discussed. Together with the Law of the Wall for rough surfaces, experimental results of mean velocity profiles are used to obtain estimates of skin-friction and the roughness function for $k^+ \approx 225 - 400$ at $Re_\tau \approx 7110 - 16700$, from which the equivalent sand-grain roughness is calculated. The method used, however, is quite sensitive to the selection of the logarithmic region considered in the regression fit, highlighting the need for an improved method to estimate roughness parameters from the mean velocity profiles. Experimental mean velocity and turbulence stress profiles also indicate the effect of roughness is primarily in the vicinity of the roughness elements, satisfying outer-layer similarity. Further evaluation of the experimental data using quadrant analysis of the sweep and ejection motions on the turbulence structures will be disseminated in future work. Mean streamwise velocity profiles, turbulence statistics, and spectral energy densities from the DNSs for $k^+ = 5, 10, 15$ and 20 at $Re_\tau \approx 190$ suggest there is a progressive departure from smooth-wall-like turbulence for all cases except the smallest roughness size investigated. We hypothesise the differences are related to the nonlinear interaction of the texture-coherent flow with the background turbulence and plan to assess the importance of this mechanism in future work. As this paper is a preliminary presentation of the results, comparisons between the experimental and numerical results will also be made in the future.

VI. Acknowledgments

The research at Cambridge has been partially supported by the Engineering and Physical Sciences Research Council (EPSRC), grant number EP/S013083/1. H.M. is supported by an award from the Cambridge Commonwealth, European and International Trust. M.J.A. was supported by EPSRC under a Doctoral Training Account, grant number EP/T517847/1. Computational resources were provided by the ‘Cambridge Service for Data Driven Discovery’ operated by the University of Cambridge Research Computing Service and funded by EPSRC Tier-2 grant EP/P020259/1. The research at Virginia Tech has been supported by the Office of Naval Research (ONR) under grants N00014-19-1-2109 and N00014-18-1-2455. The authors from Virginia Tech thank Dr. Peter Chang from ONR for this support. The authors from Virginia Tech also acknowledge the Virginia Tech Stability Wind Tunnel faculty and staff and the Aerospace & Ocean Engineering Machine Shop for their assistance during the experimental campaigns.

References

- [1] Clauser, F. H., “The Turbulent Boundary Layer,” *Adv. Appl. Mech.*, Vol. 4, 1956, pp. 1–51.
- [2] Townsend, A. A., *The Structure of Turbulent Shear Flow*, Cambridge University Press, 1956.
- [3] Chung, D., Hutchins, N., Schultz, M. P., and Flack, K. A., “Predicting the Drag of Rough Surfaces,” *Annual Review of Fluid Mechanics*, Vol. 53, No. 1, 2021, pp. 439–471.
- [4] Flack, K. A., Schultz, M. P., and Connelly, J. S., “Examination of a critical roughness height for outer layer similarity,” *Physics of Fluids*, Vol. 19, No. 9, 2007, p. 095104.
- [5] Jiménez, J., “Turbulent Flows over Rough Walls,” *Annu. Rev. Fluid Mech.*, Vol. 36, 2004, pp. 173–196.
- [6] Nikuradse, J., “Strömungsgesetze in rauhen Röhren,” *VDI-Forschungsheft*, Vol. 361, 1933, p. 1.

- [7] Bottaro, A., “Flow over natural or engineered surfaces: an adjoint homogenization perspective,” *J. Fluid Mech.*, Vol. 877, 2019, p. P1.
- [8] Fairhall, C. T., Abderrahaman-Elena, N., and García-Mayoral, R., “The effect of slip and surface texture on turbulence over superhydrophobic surfaces,” *J. Fluid Mech.*, Vol. 861, 2019, pp. 88–118.
- [9] Fritsch, D., Vishwanathan, V., Duetsch-Patel, J., Gargiulo, A., Lowe, K. T., and Devenport, W. J., “The Pressure Signature of High Reynolds Number Smooth Wall Turbulent Boundary Layers in Pressure Gradient Family,” *AIAA AVIATION 2020 FORUM*, 2020, p. 3066.
- [10] Vishwanathan, V., Fritsch, D., Lowe, T. K., and Devenport, W. J., “Analysis of Coherent Structures over a Smooth Wall Turbulent Boundary Layer in Pressure Gradient Using Spectral Proper Orthogonal Decomposition,” *AIAA AVIATION 2021 FORUM*, 2021, p. 2893.
- [11] Sharma, A., and García-Mayoral, R., “Scaling and dynamics of turbulence over sparse canopies,” *J. Fluid Mech.*, Vol. 888, 2020, p. A1.
- [12] Sharma, A., and García-Mayoral, R., “Turbulent flows over dense filament canopies,” *J. Fluid Mech.*, Vol. 888, 2020, p. A2.
- [13] Le, H., and Moin, P., “An Improvement of Fractional Step Methods for the Incompressible Navier-Stokes Equations,” *J. Comput. Phys.*, Vol. 92, No. 2, 1991, pp. 369–379.
- [14] Perry, A., and Joubert, P., “Rough-wall boundary layers in adverse pressure gradients,” *Journal of Fluid Mechanics*, Vol. 17, No. 2, 1963, pp. 193–211.
- [15] Luchini, P., “Reducing the Turbulent Skin Friction,” *Computational Methods in Applied Sciences '96*, John Wiley & Sons Ltd, 1996, pp. 466–470.
- [16] Ibrahim, J. I., Gómez-de Segura, G., Chung, D., and García-Mayoral, R., “The smooth-wall-like behaviour of turbulence over drag-altering surfaces: a unifying virtual-origin framework,” *J. Fluid Mech.*, Vol. 915, 2021, p. A56.
- [17] Pope, S. B., *Turbulent Flows*, Cambridge University Press, 2000.